Neuron 48, 789–803, June 1, 2005 ©2005 Elsevier Inc. DOI 10.1016/j.neuron.2005.09.034

Parallel Processing in Two Transmitter Microenvironments at the Cone Photoreceptor Synapse

Steven H. DeVries,[1,*] Wei Li,[1] and Shannon Saszik[1]
[1] Departments of Ophthalmology and Physiology
Northwestern University Feinberg School of Medicine
Chicago, Illinois 60611

Summary

A cone photoreceptor releases glutamate at ribbons located atop narrow membrane invaginations that empty onto a terminal base. The unique shape of the cone terminal suggests that there are two transmitter microenvironments: within invaginations, where concentrations are high and exposures are brief; and at the base, where concentrations are low and exposure is smoothed by diffusion. Using multicell voltage-clamp recording, we show that different subtypes of Off bipolar cells sample transmitter in two microenvironments. The dendrites of an AMPA receptor-containing cell insert into invaginations and sense rapid fluctuations in glutamate concentration that can lead to transient responses. The dendrites of kainate receptor-containing cells make basal contacts and respond to a smoothed flow of glutamate that produces sustained responses. Signaling at the cone to Off bipolar cell synapse illustrates how transmitter spillover and synapse architecture can combine to produce distinct signals in postsynaptic neurons.

Introduction

The design of the mammalian cone photoreceptor synapse suggests an important role for transmitter spillover. The base of the cone synaptic pedicle is ~7 μm wide and contains 20 to 40 membrane invaginations that are each ~550 nm deep and ~200 nm wide (Dowling and Boycott, 1966; Kolb, 1970). Each invagination contains an apical ribbon, which is a site of Ca^{2+}-dependent vesicle fusion (Raviola and Gilula, 1975; Zenisek et al., 2003). The postsynaptic processes are arranged in three tiers (Figure 1, inset) (Haverkamp, Grunert, and Wassle, 2000). The first tier contains the processes of two horizontal cells (HCs), which enter the invagination and ascend past the flanks of the ribbon (Raviola and Gilula, 1975). The AMPA/kainate receptors on HCs may be as close to release sites as 15–20 nm (Rao-Mirotznik et al., 1995). The second tier, located 40–240 nm beneath release sites, contains the tip of a bipolar cell that is central within the invagination (Dowling and Boycott, 1966; Raviola and Gilula, 1975; Calkins, Tsukamoto, and Sterling, 1996). In the current view, invaginating bipolar cells are depolarizing (On-center) and contain metabotropic glutamate receptors. The base of the cone terminal is carpeted by up to 500 contacts (Missotten, 1965), which comprise the third tier. At these basal contacts or junctions, cone and bipolar cell membranes abut across a narrow extracellular space (~20 nm), but there are no obvious presynaptic vesicles clusters or fusion sites (Raviola and Gilula, 1975). Hyperpolarizing (Off-center) bipolar cells contain AMPA or kainate receptors (DeVries, 2000) and are said to contact cones exclusively in the basal position (Kolb, 1979), 110–1840 nm from the nearest ribbon sites (Calkins et al., 1996). While the ultrastructure suggests that cone transmitter could sequentially spill over three tiers of contacts, this sequence and its functional consequences have yet to be established.

Possible roles for spillover come from considering two functions of the cone synapse: the transmission of small, graded light responses and the initiation of parallel signal processing. Cones rest at −40 to −45 mV in the dark (Baylor and Fuortes, 1970), where a sustained Ca^{2+} current maintains a steady rate of transmitter release (Ashmore and Copenhagen, 1983; DeVries and Schwartz, 1999). A flash of light produces a slow membrane hyperpolarization that is graded in amplitude with intensity (Baylor and Fuortes, 1970), suppressing both Ca^{2+} influx and transmitter release. The quantization of release is characteristic of transmission at chemical synapses, but the noise produced by a continuous rain of quanta in the dark could interfere with the transmission of the small signals produced by dim lights. This is clearly not the case, since hyperpolarizations in turtle cones as small as 100–250 μV can alter behavior and must therefore be transmitted to postsynaptic neurons (Fain et al., 1977; Dvorak et al., 1980). In On bipolar cells, quantal events can be filtered by a slow postsynaptic second messenger cascade (Sampath and Rieke, 2004). In Off bipolar cells, the membrane time constant may attenuate rapid quantal currents more than slower light responses (Ashmore and Copenhagen, 1983). Membrane filtering, however, may be limited by the small size of some Off bipolar cells and a low membrane resistance during steady glutamate exposure. We propose an additional filtering mechanism in which an extended distance between ribbon release sites and basal contacts allows diffusion to temporally smear quantal events, thereby reducing the steady noise in small Off bipolar cells. Miniature synaptic events have been observed in salamander Off bipolar cells (Maple et al., 1994; Cadetti et al., 2005), but salamander and mammalian cone synapses are differently organized (Lasansky, 1973).

The cone synapse is also a site of parallel signal processing. An individual cone contacts both On and Off bipolar cells, which are further divided into 8 to 12 subtypes based on their level of termination within the inner plexiform layer (IPL). Ultrastructural studies suggest that some Off bipolar cell subtypes tend to contact cones near the mouths of invaginations, whereas others appear to have no preference for contact location (Kolb, 1970; Nelson and Kolb, 1983; Hopkins and Boycott, 1992, 1997). The observation that Off bipolar cell contacts may be spatially organized relative to invaginations raises the possibility that these contacts could sample the spatiotemporal glutamate concentration profile at different points. Differences in sampling distance could produce distinct signals in different Off bipolar cells.

*Correspondence: s-devries@northwestern.edu

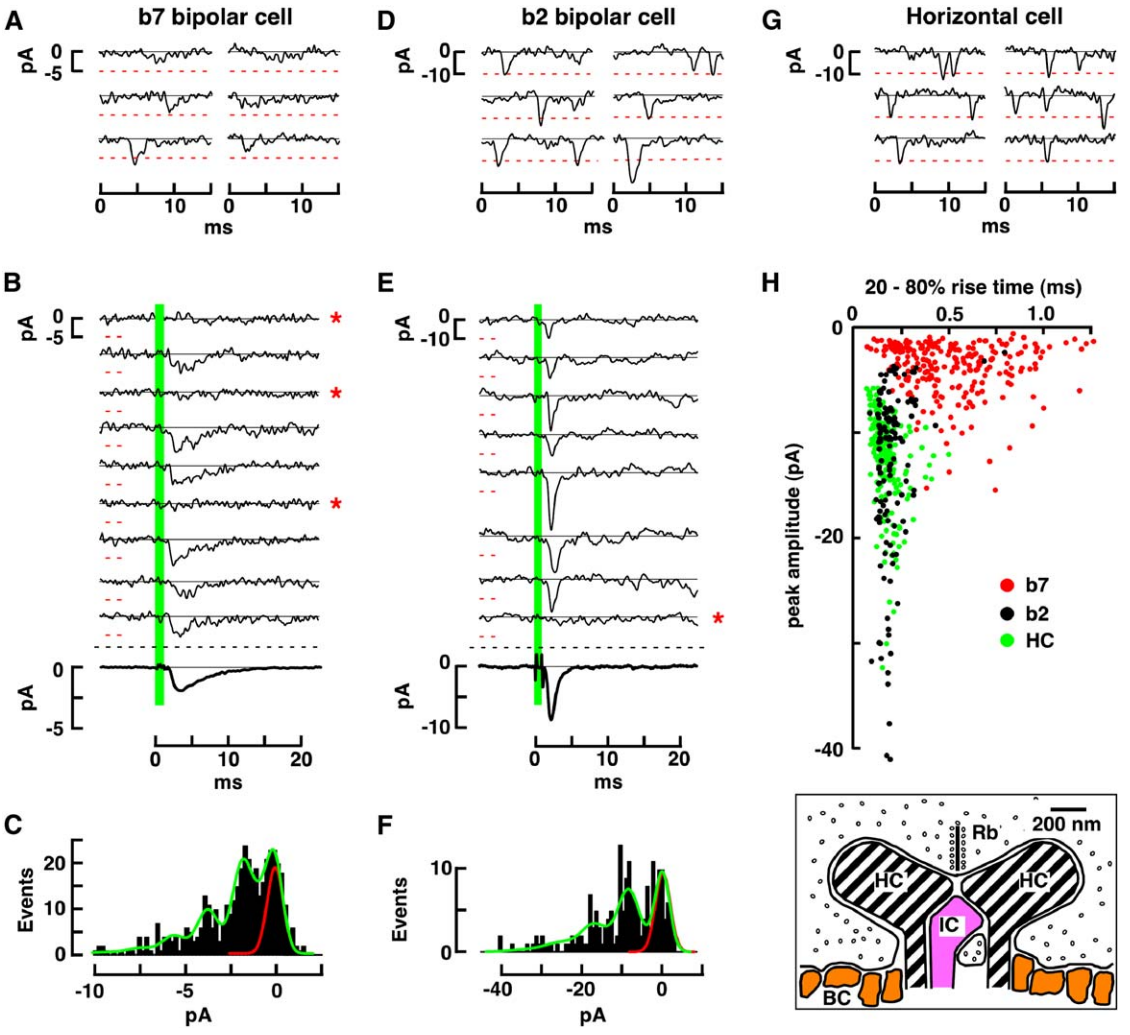

Figure 1. Spontaneous and Evoked Events in Off Bipolar and Horizontal Cells

(A) Spontaneous activity in a b7 bipolar cell maintained at a membrane voltage of −70 mV.

(B) Consecutive traces from the same bipolar cell during a brief (0.9 ms) cone depolarization (green bar) in the loose seal configuration. Asterisks denote apparent response failures. Bottom trace shows the ensemble average.

(C) All-event amplitude histogram. The green curve was obtained from the "2-release site" fit and predicts event amplitudes of −1.9 and −0.6 pA. The red curve shows the distribution of response failures calculated from the two-site fit (Gaussian width, 0.44 pA; mean, −0.06 pA). The major event accounted for 76% of all events.

(D–F) Spontaneous and evoked events in a b2 cell. The cone was depolarized in the loose seal configuration. The fit to the amplitude histogram indicates that a large event (−8.5 pA) comprised all but 5% of the events.

(G) Spontaneous events in a HC.

(H) Plot of peak amplitude versus rise time for the evoked events in the b2 and b7 cells and the spontaneous events in the HC. (Inset) Diagram of an invagination and surrounding region showing the ribbon (Rb), HCs, central invaginating contact (IC), and basal contacts (BC).

We have investigated transmission at the cone to Off bipolar cell synapse in slices from the cone-dominant ground squirrel retina (*Spermophilus tridecimlineatus*). In violation of a general rule concerning the basal location of Off bipolar cell contacts, we show that one subtype of Off bipolar cell makes cone contacts that are functionally central-invaginating, whereas two other types make classical basal contacts. The invaginating Off bipolar cell is exposed to rapid swings in glutamate concentration that facilitate transient responses, whereas, in the cells that make basal contacts, quantal events are temporally filtered by diffusion, leading to a smoothing of the ongoing current noise and sustained responses.

Results

Spontaneous and Small Evoked Events in Off Bipolar Cells

Transmitter diffusion can shape quantal events. Qualitatively, quantal responses should be large and fast if release sites and receptors are juxtaposed across a narrow synaptic cleft. Conversely, if release sites are remote from receptors, as would be the case if transmitter were diffusing from ribbons to basal contacts, then quantal events should be small and smeared in time. Events were examined in three subtypes of ground squirrel Off bipolar cells, the b2, b3, and b7 (West, 1976; Linberg et al., 1996; DeVries, 2000). For comparison, events

Table 1. Parameters of Small Evoked EPSCs

Cell	Peak (pA)			Rise (ms)		n
	Ampl. Histo.	Var./Mean	Failures	Median	Mean	
b2	−9.9 ± 2.4	−12.0 ± 1.7	−8.5 ± 1.6	0.20 ± 0.02	0.22 ± 0.02	5
b3	−2.1 ± 0.7	−2.2 ± 0.9	−1.7 ± 0.7	0.74 ± 0.14	0.89 ± 0.09	4
b7	−2.4 ± 0.4	−2.6 ± 0.9	−1.8 ± 0.5	0.68 ± 0.27	0.73 ± 0.30	6

also were recorded in HCs. All four cell types use AMPA/kainate receptors, but the processes of HCs clearly abut ribbon release sites within invaginations. As expected, b3 and b7 cells had quantal events that were small and slow. Surprisingly, b2 cells had events that were relatively large and fast and comparable in shape to those in HCs.

We measured postsynaptic currents during both spontaneous release (spontaneous EPSCs) and release evoked by a small, brief cone depolarization (small evoked EPSCs). Spontaneous events were recorded in a b7 cell (Figure 1A), reflecting input from several cones. Figure 1B shows consecutive traces from the same b7 bipolar cell following a brief depolarization in a single presynaptic cone. The sequence contains both small EPSCs and response failures, consistent with the idea that some of the events are uniquantal. The amplitudes and shapes of the spontaneous and small evoked EPSCs are similar. The average evoked event (Figure 1B, bottom; 440 consecutive traces) had a peak of −1.9 pA and a 20%–80% rise time of 0.51 ms. A peak amplitude histogram (Figure 1C) shows both response failures and peaks at one or more amplitudes. While distinct peaks were apparent, their interval did not correspond to a fixed unit. Instead, an adequate fit to the histogram was obtained by assuming that the unitary events had two different amplitudes (see Experimental Procedures). Although no mechanism is implied, one can think of larger and smaller events as originating at ribbons that are nearer and farther from the bipolar cell cone contact. The fit to the histogram in Figure 1C predicted event amplitudes of −1.9 and −0.6 pA. The existence of the smaller amplitude event was inferred solely from the fitting procedure and could not be verified by direct inspection. Estimates of quantal amplitude were also obtained by calculating the ratio between the ensemble variance and mean (−3.4 pA) and by assuming Poisson release statistics and using the fraction of response failures (−1.8 pA; 151 failures). Both measures made the simplifying assumption that there was only a single event size. We observed similar responses in four b3 and six b7 cells (Table 1). The results suggest that unitary events in b3 and b7 cells are relatively small and slow.

A similar experiment was performed at a cone to b2 cell synapse. Both spontaneous (Figure 1D) and small evoked (Figure 1E) events had rapid time courses, with the average event in Figure 1E having a rise time of 0.30 ms and a peak amplitude of −8.5 pA (Figure 1F) (amplitude from variance/mean = −9.9 pA, from response failures = −6.7 pA; 190 consecutive events with 53 failures). We observed similar responses in a total of five b2 cells (Table 1). For comparison, spontaneous events were recorded in an HC (Figure 1G). The scatter plot in Figure 1H compares the events in all three cell types. In general, the rise times and amplitudes of the horizontal and b2 cell events were similar, and both were faster and larger than the events in the b7 cell.

The differences in event shape were not an artifact of selection or a consequence of damage to the synaptic contact. We stimulated a cone and recorded simultaneously from two postsynaptic bipolar cells, either a b2 and a b3 or a b2 and a b7 (Figure 2). The EPSC in the b2 cell was characteristically fast, with a rise time similar to that of the b2 cell response in Figure 1E. The responses in the b3 and b7 cells were slower, with rise times similar to that of the b7 cell response in Figure 1B. It is unlikely that damage to the synapse could have produced slow responses in b3 and b7 cells while sparing the responses of b2 cells, since the processes of all three types commingle at the terminal.

Presynaptic Mechanisms and Quantal Response Shape

The mechanisms that could produce different quantal response shapes fall into three categories: presynaptic, postsynaptic, and cleft. Examples from each category

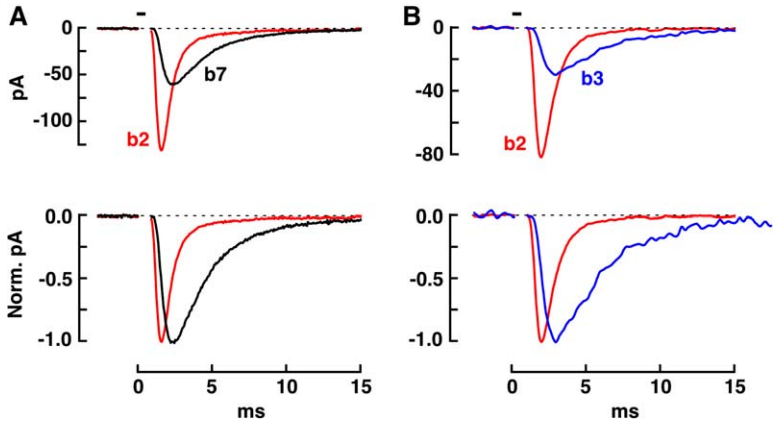

Figure 2. A Brief Cone Depolarization (0.6 ms) Produced Medium-Sized EPSCs with Different Time Courses in Two Postsynaptic Bipolar Cells

(A) A b2 (rise time, 0.26 ms; maximal response in a subsequent series, −222 pA) and a b7 (0.42 ms and −197 pA) cell. Normalized responses shown below. Cone depolarized (horizontal black bar) in the loose seal configuration.

(B) A b2 (0.31 ms and −140 pA) and a b3 (0.56 ms and −59 pA) cell. Cone depolarized in the whole cell configuration from −70 to −20 mV.

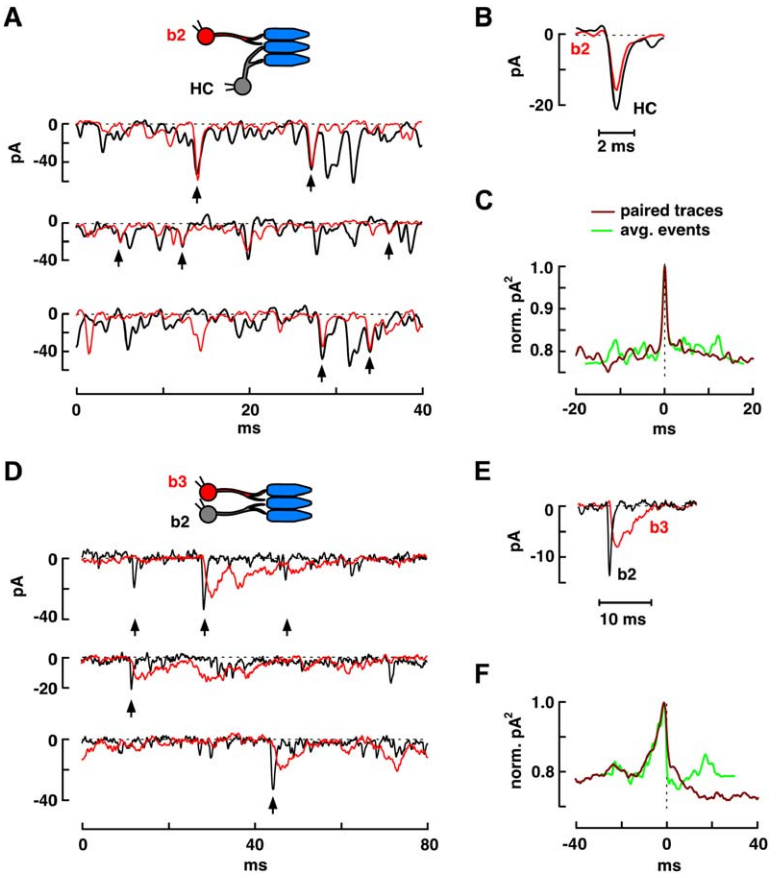

Figure 3. Correlated Spontaneous Events in Off Bipolar and HCs

(A) Simultaneous membrane currents recorded in a b2 (red traces) and HC (black traces). Arrows denote contemporaneous events. Larger events were selected for illustration since they are more easily distinguished from background activity.

(B) Selected events were excised, aligned by their leading edge, and averaged.

(C) Cross-correlation plots obtained from the paired traces in (A) (brown line) and the averaged events in (B) (green line). Plots were normalized to facilitate comparison of peak shape.

(D) Simultaneous membrane currents recorded in a b2 and a b3 cell.

(E) Select events aligned and averaged.

(F) Normalized cross-correlation plots.

include different vesicle release pools, different postsynaptic receptor kinetics, and differences in transmitter diffusion distance, respectively. Presynaptic mechanisms were considered first.

Response shapes might differ if b2 and HCs on the one hand and b3 and b7 cells on the other receive transmitter from different pools of vesicles with, for example, fusion pores that open at different rates. Both pools could be ribbon associated, representing different priming states of fusion-competent vesicles, or one pool might be ribbon independent or ectopic (i.e., basal; Zenisek et al., 2003; Matsui and Jahr, 2003). The following results, however, suggest that transmitter from a single vesicle or release event can simultaneously produce both fast and slow EPSCs in different bipolar cells.

We recorded from pairs of postsynaptic neurons in various combinations under conditions of spontaneous release. The traces in Figure 3A show the simultaneous currents in a b2 and an HC. The close timing of two spontaneous events (Figure 3A, arrows) suggests that the events are produced by the release of a single vesicle (or a linked group of vesicles; Singer et al., 2004) at a cone terminal that is contacted by both bipolar cells. Frequently, events occurred in one cell and not the other. This was anticipated, since the populations of cones sampled by the two postsynaptic cells would not entirely overlap. The occurrence of paired events in excess of chance was confirmed by cross-correlating the currents from the two cells (Figure 3C). The cross-correlation plot had a central peak the width of which closely matched that of the peak obtained by cross-correlating isolated and averaged events from each cell (Figures 3B and 3C). By comparing the areas under the peaks of the curves in Figure 3C prior to normalization, it was possible to estimate the joint event rate in excess of chance (64 s^{-1}; the average single event rate for both cells was 434 s^{-1}). The significance of the central peak was confirmed by shuffling the traces in one of the cells and then repeating the cross-correlation (data not shown). The significance of the central peak can also be inferred from the relatively small size of the fluctuations on the flanks of the cross-correlation plot. Figures 3D–3F show similar results for fast and slow events in a b2 and a b3 cell (joint event rate = 26 s^{-1}; average single event rate = 184 s^{-1}). Joint events were observed in the following cell combinations: b2 and b3 (n = 4 pairs), b3/7 and b3/7 (1), b2 and b7 (1), HC and b2 (2), HC and b3/7 (3), and HC and b3 (1). The designation b3/7 arises because b3 and b7 cells could not be distinguished in the absence of axons that were frequently cut prior to recording to reduce membrane noise. The results are consistent with the idea that vesicles from a single pool can produce the characteristic temporal events observed in each of the cell types. Since glutamate receptors on HC dendrites are near ribbon fusion sites (Haverkamp et al., 2000, 2001a), we infer that this pool is ribbon associated.

Postsynaptic Mechanisms and Quantal Response Shape

The different quantal response shapes could be produced by differences in receptor kinetics (Cossart

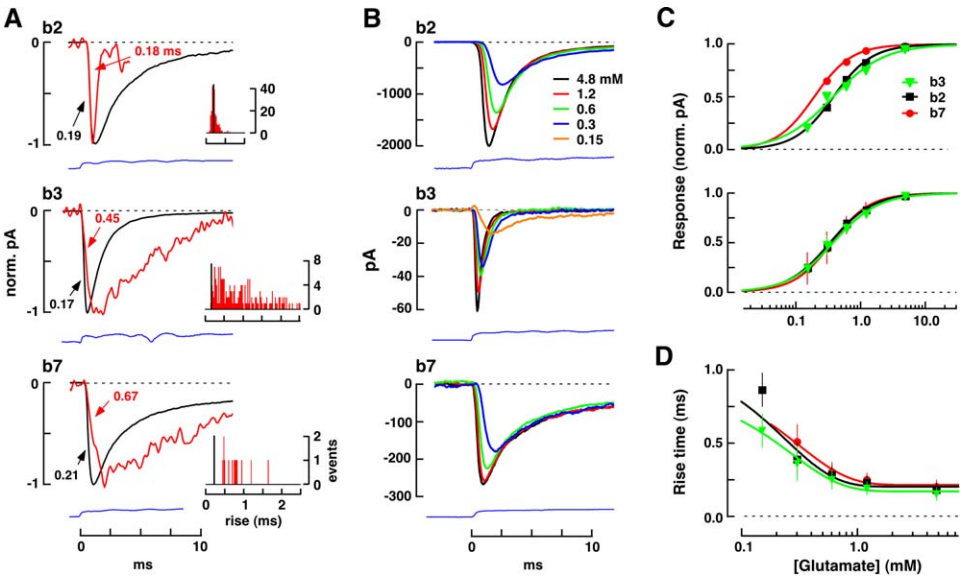

Figure 4. The Time Course and Concentration Dependence of Receptor Activation

(A) b2, b3, and b7 cell receptors were rapidly switched to a solution that contained 4.8 mM glutamate. Normalized receptor currents are shown above (black traces) and the timing of the solution switch below (blue traces). Peak response amplitudes prior to normalization were as follows: b2, −2190 pA; b3, −1850 pA; and, b7, −1170 pA. Average spontaneous EPSCs obtained prior to removing the bipolar cell from the slice were normalized and superimposed (red traces). Amplitudes prior to normalization were as follows: b2, −14.8 pA (average of eight representative events); b3, −4.7 pA (16 events); b7, −4.6 pA (nine events). Current traces are labeled with 20%–80% rise times. (Insets) All-event rise-time histograms of the spontaneous EPSCs (red bars) and the receptor response (black bar).

(B) Receptor responses to different concentrations of glutamate. Bottom traces (blue) show the timing of the solution switch.

(C) (Above) Plot of normalized response versus glutamate concentration for the three cells in (A). The EC_{50}s and Hill coefficients for the b2, b3, and b7 cells were 384 μM and 1.46, 380 μM and 1.10, and 195 μM and 1.50, respectively. Points are the average of up to three separate determinations. (Below) Plot of average response versus glutamate concentration for each cell type (three b2, five b3, and six b7 cells). Results from individual cells were normalized prior to averaging.

(D) Plot of response rise time versus glutamate concentration. Data points were fitted with exponential curves. Limiting rise times at high glutamate concentrations were 0.19 ± 0.02, 0.16 ± 0.05, and 0.21 ± 0.03 ms for b2, b3, and b7 cells, respectively. Results from four b3 cells (including one nucleated patch), five b7 cells (including one nucleated patch), and a single b2 cell recorded as a nucleated patch (b2 cell data points are the average of three to six determinations). The rise time of the solution switch in this group of experiments was 0.19 ± 0.04 ms.

Error bars show the standard deviations.

et al., 2002): HCs and b2 bipolar cells use AMPA receptors to receive the cone signal, whereas b3 and b7 cells use kainate receptors. However, as will be shown below, differences in receptor kinetics alone cannot account for the differences in quantal time course.

It was first useful to compare the rise times of spontaneous EPSCs with the minimal rise times of the isolated receptors in the same cells. Spontaneous events in b2, b3, and b7 cells were first recorded in a slice. Rise times were analyzed in two ways: first, by aligning selected events according to their leading edges and averaging (Figure 4A); and second, by plotting all-event histograms (Figure 4A, insets). Minimal receptor rise times were then obtained by removing the cell from the slice and rapidly applying a high concentration of glutamate (4.8 mM; Figure 4A; DeVries, 2000). We found that the rise times of all three receptors were comparably fast (0.17–0.21 ms) when exposed to 4.8 mM glutamate. In addition, for both the b3 and b7 cells, the receptor rise time was consistently faster than that of the spontaneous EPSC. For the b2 cell, the rise times of some spontaneous EPSCs slightly exceeded that of the receptor, which suggests that the measured receptor rise time was limited by the solution switching speed. We conclude that if differences in receptor kinetics are responsible for fast and slow quantal events, they may only be evident at submaximal glutamate concentrations.

When exposed to submaximal concentrations, glutamate receptor rise times slow (Hausser and Roth, 1997). If b2, b3, and b7 receptor rise times slow with a different concentration dependence, then a single postsynaptic glutamate concentration profile might produce both fast and slow quantal responses. Divergence would be likely if, for example, the glutamate affinity of the AMPA receptor exceeds that of the kainate receptors. Receptor responses were measured during steps into solutions that contained different glutamate concentrations (Figure 4B). Peak response was plotted against concentration for both the individual cells from Figure 4B and the cell populations (Figure 4C, above and below). Fits to the data showed that the half-maximal responses (EC_{50}) for all three receptors occurred within a narrow range of glutamate concentrations (339–375 μM; Table 2).

The relationship between glutamate concentration and receptor rise time was directly measured during a subset of experiments that were optimized for rapid solution exchange (Figure 4D). The responses of all three receptor types attained limiting rise times of ~0.2 ms in 4.8 mM glutamate. Concentrations of glutamate below

Table 2. Properties of Isolated Receptors

	b2	b3	b7
20%–80% Rise (ms)[a]	0.26 ± 0.15	0.21 ± 0.06	0.26 ± 0.11
Desensitization (ms)			
τ_1	1.3 ± 0.8 (74%)	1.3 ± 0.5 (80%)	1.4 ± 0.4 (73%)
τ_2	8.9 ± 5.8	8.9 ± 7.2	9.0 ± 3.1
Deactivation (ms)			
τ_1	0.8 ± 0.2 (59%)	1.2 ± 0.6 (60%)	1.5 ± 0.7 (82%)
τ_2	7.8 ± 6.1	10.2 ± 5.6	17.8 ± 14.4
Steady/peak (%)	4.2 ± 1.8	2.8 ± 1.4	9.2 ± 5.5
Cells	4	13	9
EC_{50}	339 ± 35	370 ± 93	375 ±149
Hill coef.	1.40 ± 0.14	1.28 ± 0.19	1.51 ± 0.26
Cells	4	7	7

[a] 4.8 mM glutamate.

1 mM produced progressively slower rise times. Overall, the rise time versus concentration plots for the three cell types were similar, and very close to the plot obtained from a more extensive sampling of AMPA receptors in rat cerebellar purkinje cells (Hausser and Roth, 1997). It is evident from Figure 4D that there is no single glutamate concentration that can simultaneously produce both the ~0.2 and ~0.6 ms rise times that are characteristic of b2 and b3/b7 small events, respectively. The results are consistent with the idea that receptor kinetics alone cannot account for the different quantal time courses. However, if receptors are exposed to different concentrations of glutamate during a synaptic response, as might occur if they are located at different distances from release sites, then the rise times of the more distant receptors could be further slowed by the concentration dependence of activation.

Cleft-Related Mechanisms and Quantal Response Shape

The rapid activation and deactivation kinetics of the b3 and b7 cell receptors (Table 2) suggests that receptor activity during a small or spontaneous EPSC should coincide with the presence of glutamate in the cleft near receptors. Nonetheless, we wanted to specifically exclude the possibility that the temporally smeared b3/b7 cell response is caused by receptors that bind glutamate tightly during a concentration transient and then remain active for several milliseconds after transmitter has ebbed from the cleft (Lester et al., 1990).

We used the weak antagonist kynurenic acid (KYN) to probe for the presence of glutamate late in the b3/b7 cell synaptic response. At equilibrium with a population of receptors, KYN has a significant probability of unbinding over the time interval of an EPSC to reveal "fresh" receptors (Diamond and Jahr, 1997). The constant production of fresh receptors allows the population to respond to changes in glutamate concentration that might otherwise be obscured by receptor kinetics or saturation (Clements et al., 1992; Diamond and Jahr, 1997). Two prominent effects of weak antagonists are their ability to slow the apparent rise of an EPSC and their decreased effectiveness as progressively stronger presynaptic stimuli lead to higher concentrations of cleft glutamate under conditions of multivesicular release (Tong and Jahr, 1994; Diamond and Jahr, 1997). Both effects were observed when 0.5–1.5 mM KYN was applied at the cone to b3/b7 cell synapse (see Figure S1 in the Supplemental Data available online). Weak antagonists can also produce characteristic effects late in a synaptic response: As the local glutamate concentration decreases, KYN may quicken the falling phase of an EPSC by rebinding to newly vacated receptors, precluding receptor reactivation by any glutamate that might loiter in the cleft (Liu et al., 1999). This competition is useful for demonstrating the presence of cleft glutamate late in a synaptic response.

We measured the effect of KYN on b3 cell EPSCs (Figure 5A). The experiment began with a control (Figure 5Ba). Strong antagonists like DNQX and NBQX unbind receptor slowly and should reduce EPSC size without changing EPSC shape. Initially, a series of brief cone depolarizations produced EPSCs with a mean peak amplitude of −13 pA. DNQX (2 μM) reduced EPSC amplitude by 73%, while having little effect on EPSC shape (the time constant, τ, obtained by fitting the response decay with an exponential curve, decreased by 5%). In a total of nine experiments on b3 and b7 cells, DNQX or NBQX (2–10 μM) decreased peak EPSC amplitude by 73% ± 15% and slightly increased the response decay time ($\Delta\tau$ = 10% ± 24%). Next, the presynaptic cone depolarization was increased, producing an EPSC with a peak amplitude of −25 pA (Figure 5Bb). KYN (1.5 mM) reduced EPSC amplitude by 86%, slowed EPSC rise (peak shift = 0.61 ms), and produced an obvious quickening of the decay (τ decreased by 28%). Finally, the amplitude of the cone depolarization was decreased, leading to an EPSC with a mean amplitude of −14 pA (Figure 5Bc), similar to that of the EPSC in Figure 5Ba. KYN reduced the EPSC amplitude by 88% and also slowed the rise (peak shift = 0.57 ms) and quickened the response decay (τ decreased by 20%), although to a lesser extent then for the larger response in Figure 5Bb. Overall, KYN (0.2–1.5 mM) reduced the EPSC decay τ in b3 and b7 cells by 20% ± 6% (n = 9; the decrease was significant when compared to the effect of DNQX or NBQX, t test, $p < 0.006$). The effect of KYN on the EPSC decay is consistent with the idea that glutamate and KYN compete for b3/b7 cell receptors late in the EPSC time course. The results argue against the notion that transmitter is present in the cleft only briefly but produces smeared responses by binding tightly to receptors initiating a long-lived active state.

The Effect of Glutamate Transporters on EPSC Shape

Cones contain glutamate transporters (Eliasof and Werblin, 1993), and glutamate transporters can alter cleft glutamate during an EPSC by both rapid binding and delayed unbinding (Diamond and Jahr, 1997). We tested for an effect of glutamate transporters on EPSC shape by blocking transport with the competitive antagonist DL-*threo*-β-benzyloxyaspartic acid (TBOA, 25–100 μM; Wadiche and Jahr, 2001). TBOA increased the mean

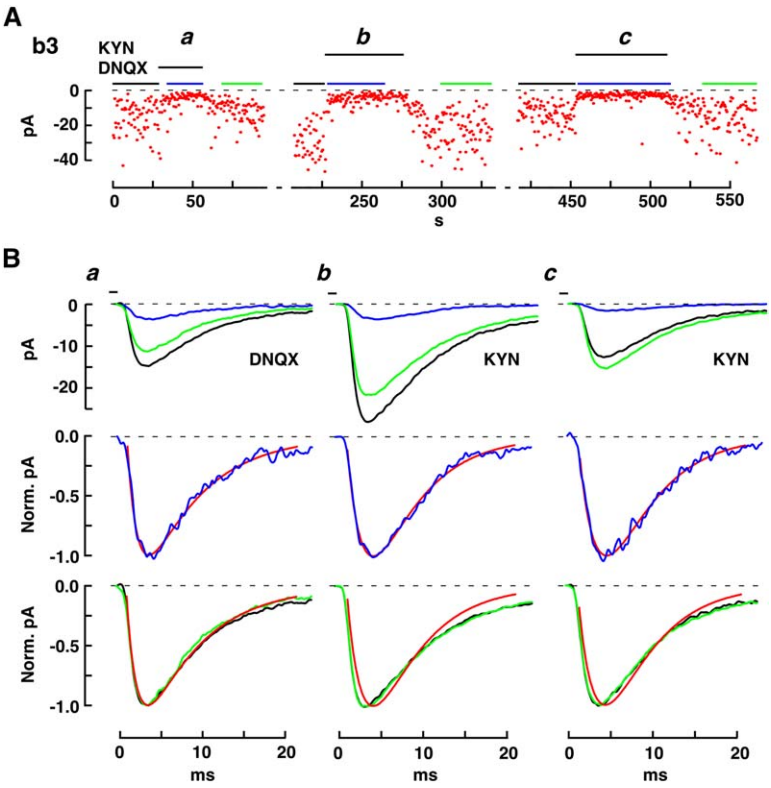

Figure 5. Competition between KYN and Glutamate for Receptor Occupancy Changes the Decay of b3 Cell EPSCs

(A) Plot of b3 cell EPSC peak amplitude versus time during a series of brief cone depolarizations. Black horizontal bars (above) show the interval of application of either 1.5 mM KYN or 2 μM DNQX. Dashes along the abscissa denote intervals during which the amplitude of the cone depolarization was varied. The maximum amplitude of the EPSC was −70 pA.

(B) (Top row) Average EPSCs during the intervals denoted by the black, blue, and green horizontal lines and *italicized* letters in (A). Timing of the cone depolarization is indicated by a horizontal black bar (duration, 0.6 ms). (Center row) Average EPSC in drug solution normalized and fitted with a curve obtained from Equation (2) (red line). (Bottom row) Normalized EPSCs in control and fits to the normalized EPSCs in drug.

duration (measured as the peak width at half-height) of b3/b7 EPSCs by 37% ± 19% (n = 10). TBOA also produced a marginal increase in b2 EPSC width (4% ± 4%, n = 5). TBOA increased the difference between the widths of b2 and b3/b7 EPSCs, which strongly suggests that transporters are not responsible for creating the fast and slow quantal responses.

Confocal Imaging of the Cone Pedicle

By excluding likely pre- and postsynaptic mechanisms, the results so far suggest that the organization of the synaptic cleft may account for the differences in response shape. In this view Off bipolar cell contacts are segregated at the cone pedicle, with b2 contacts closer to invaginations and b3 and b7 contacts more distant. Consequently, we used confocal microscopy to image the locations of the contacts between pre- and postsynaptic cells after injecting each with a different fluorescent tracer. We also used antibodies to label pedicle landmarks. The first task was to establish a marker for invaginations. Light microscopic studies in the primate and rodent retinas showed that labeling for the AMPA receptor subunits GluR2–4 is punctate and situated near ribbons within invaginations. Immunoelectron microscopy further localized these subunits to the invaginating dendrites of HCs (Morigiwa and Vardi, 1999; Haverkamp, Grunert, and Wassle, 2000, 2001a).

We confirmed that AMPA receptor subunit labeling can be used as a marker for invaginations in ground squirrel cones. Tracer-injected cones (Figures 6A and 6C) displayed distinct terminal indentations. Evidence that the indentations corresponded to invaginations came from counting the number (15.0 ± 2.4 per terminal compared to 15 measured by electron microscopy in the ground squirrel, and about 20 in the central primate retina; West and Dowling, 1975; Haverkamp, Grunert, and Wassle, 2001a). Labeling for the GluR2/3 subunit of the AMPA receptor was strongest at the upper end of an indentation, corresponding to the presumptive region of vesicle fusion, and trailed off toward the lower end, only rarely emerging past the apparent basal surface (Figures 6B and 6D). As expected, cone ribbons, labeled with an antibody to RIBEYE, were closely associated with the putative AMPA receptor clusters (Figure 6E). An antibody to the GluR4 subunit labeled with a similar pattern; an antibody to the GluR1 subunit did not label the ground squirrel retina. The results suggest that the GluR2/3 subunit can serve as a marker for invaginations in ground squirrel cones.

We next determined the spatial relationship between the cone contacts of b2, b3, and b7 cells and the AMPA receptor labeling within invaginations. Figure 6F shows the dendrite of an injected b2 bipolar cell that curved beneath the surface of a cone pedicle giving off several twigs that ended in the AMPA receptor clusters. In contrast, the processes of injected b3 and b7 cells appeared to terminate along the cone base and did not overlap with AMPA receptor clusters (Figures 6G and 6H). The different sites of dendrite termination were most apparent when b2 and b3/b7 cells were injected and AMPA receptors labeled at the same time (Figures 6I–6K). Flat-mount views also showed that b2 cell dendrites consistently ended in the vicinity of AMPA receptors while b3 and b7 contacts ended in-between (Figures 6L and 6M). We conclude from the anatomy that b2 cell dendrites are associated with invaginations, whereas b3 and b7 cell dendrites contact the cone pedicle between invaginations along its basal surface. Due to the

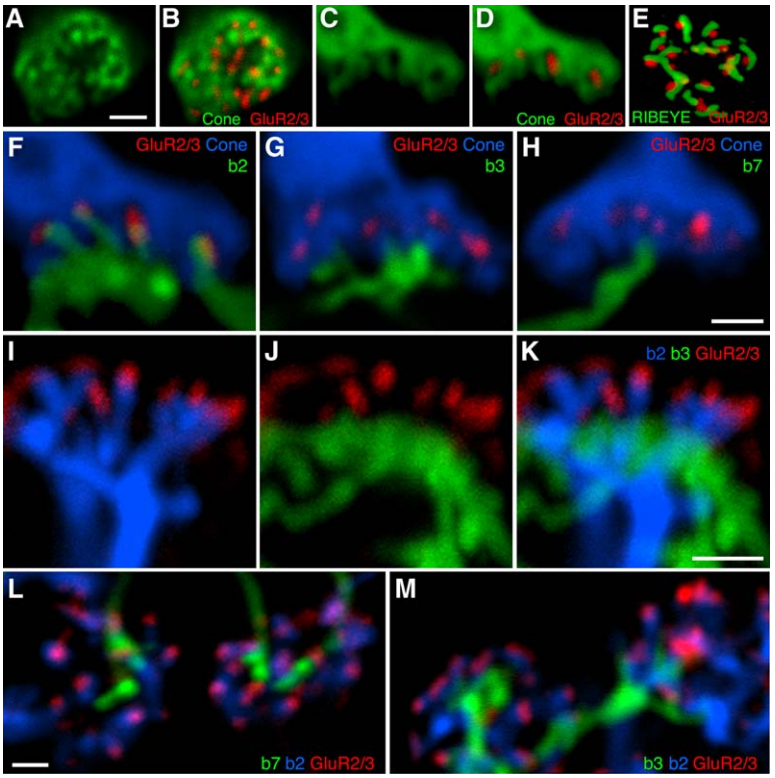

Figure 6. Locations of the Dendritic Contacts of b2, b3, and b7 Cells Relative to Cone Invaginations

(A–D) Cones were labeled by injection with Alexa 488 (green) and immunostained for the AMPA receptor GluR2/3 subunit (red).

(A and B) Flat-mount view. The interinvagination distance was 0.67 ± 0.15 μm (n = 64).

(C and D) Cross-sectional view. The invagination depth was 0.48 ± 0.09 μm (n = 106).

(E) Flat-mount view of a cone terminal labeled with an antibodies to the ribbon marker RIBEYE (green) and the GluR2/3 subunit (red).

(F–H) Cross-sectional views showing cones (blue) and b2, b3, and b7 bipolar cells (green) stained by tracer injection. AMPA receptor subunits (red) are localized to invaginations.

(I–K) Tracer injections into a b2 (blue) and a b3 (green) bipolar cell. Immunostaining of AMPA receptors (red). The three panels contain the same terminal.

(L and M) Flat-mount view showing dendritic terminations of injected b2 (blue) and b3 or b7 (green) bipolar cells relative to GluR2/3 labeling. Different cones in each panel. Scale bar, 1 μm.

limited resolving power of the light microscope, it was not possible to distinguish whether b2 cell dendrites are fully invaginating as a central element or merely semi-invaginating, meaning that they insert partway into an invagination around its periphery (Kolb, 1970).

The Effect of Synapse Organization on Signal Transmission

A continuous rate of vesicle fusion in the dark might be expected to produce a continuously fluctuating membrane current in postsynaptic cells. We first simulated the impact of unitary events on the continuous bipolar cell noise. Figure 7A, inset, shows actual b2 (fast) and b3 (slow) small events scaled to have the same integral (i.e., charge transfer), −7.4 fC. The rationale for the scaling will be discussed below. Figure 7A also shows the simulated current response in postsynaptic b2 and b3 cells during the temporally random arrival of vesicles at an average rate of 750 s^{-1}. This rate will also be justified below. Since the charges transferred during the b2 and b3 cell events are equal, the mean current is the same for both cells (−5.6 pA). However, the current fluctuations are different. The square root of the noise variance (σ) of the b2 cell exceeds that of the b3 cell by 3-fold.

We next compared the properties of simulated and recorded synapses. Figure 7B shows current traces obtained from a b2 and a b3 cell while the presynaptic cone was maintained at either −70 mV or a depolarized voltage that maximized release (−35 mV for the b2 cell and −5 mV in loose seal mode for the b3 cell). Bipolar cell current traces were relatively quiescent when the cone was held at −70 mV, as few quanta are released. During cone depolarization and continuous release, the impact of individual quanta on the membrane current can be readily discerned in b2 cells, whereas the smeared events in b3 cells merge together to produce a relatively even trace.

The steady release rate onto a bipolar cell equals the mean synaptic current divided by the charge transferred during the average quantal event. Because receptor desensitization may occur during steady release, the size of the component quantal events may differ from that measured under nondesensitizing conditions (e.g., in Figure 1), leading to an underestimate of the release rate. The mean event rate can be estimated by an alternative approach that does not require information about the extent of receptor desensitization. This approach uses the small EPSC profile (Figure 7A, inset), Campbell's theorem [Equation (1); Rice, 1944], and the measured increase in the current mean ($\Delta\bar{x}$) and variance ($\Delta\sigma^2$) during

$$\frac{\Delta\sigma^2}{\Delta\bar{x}} = \frac{\int F^2(t)dt}{\int F(t)dt} \quad (1)$$

the steady cone depolarization, where F(t) represents the scaleable time course of the quantal event and the integral is over the event interval. For the b3 cell, the mean event amplitude was calculated from Equation (1) to be −1.1 pA (charge = −7.4 fC) and the vesicle "impact" rate 662 vesicles s^{-1}. The −1.1 pA event amplitude is about 2-fold smaller than the unitary event amplitude obtained by measuring the mean and variance of small evoked EPSCs in the same pair. The amplitude reduction is reasonably attributed to postsynaptic kainate receptor desensitization during continuous glutamate release, since b3 kainate receptors recover very slowly from desensitization ($\tau \approx 1.5$ s; DeVries, 2000). The steady quantal detection rate is probably still an underestimate since, for simplicity, channel noise has been

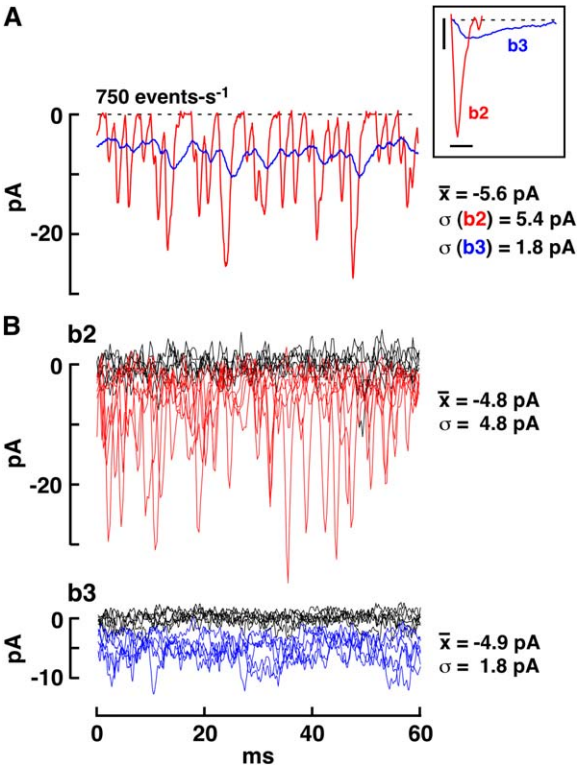

Figure 7. Properties of Continuous Signaling at the Cone Synapse

(A) Simulation of the steady current at a cone to b2 and a cone to b3 cell synapse. Quantal events (see inset) were distributed randomly in time at a mean rate of 750 events s^{-1} and the event profiles summed. (Inset) Average small evoked EPSCs from the bipolar cells in (C) were scaled to account for receptor desensitization during continuous release (scale bars, 2 pA and 2 ms).

(B) Voltage-clamp recordings from a b2 and a b3 cell (separate experiments). Initially, the cone was maintained at a hyperpolarized voltage to simulate conditions in light (black traces). Subsequently, cone voltage was maintained at a depolarized level simulating dark (red and blue traces). The mean current increase when the cones were depolarized is similar for both cells, whereas the noise standard deviation (σ) is very different.

disregarded. Taking channel noise (unpublished data) into account nearly doubles the event rate and halves the event size. A similar analysis of the steady b2 current resulted in a calculated unitary event amplitude of −6.8 pA (charge = −6.3 fC) and an event rate of 750 vesicles s^{-1} (the −6.3 fC event was scaled to −7.4 fC for the purpose of illustration in Figure 7A). Adjusting for receptor noise increased the event rate by 15%. The peak amplitude of the b2 cell event during steady cone depolarization was about two-thirds of that typically measured following a brief cone depolarization (−6.8 versus −8.5 to −12 pA, Table 1), presumably due to a receptor desensitization that carries over from one event to the next. Similar event rates and amplitudes were obtained in one additional b2 and three b3 cells. Both simulated and actual results show that steady transmission under dark conditions is noisier in b2 cells than in b3 cells and suggest that postsynaptic receptors are up to 50% desensitized during steady release, which occurs at a rate of 500–1000 vesicles s^{-1}.

Bipolar cell membrane resistance (*R*) and capacitance (*C*) acting in parallel can filter synaptic currents. Thus, a membrane time constant ($\tau = RC$) that is long relative to the quantal event duration may reduce the difference between the *voltage* fluctuations in b2 and b3/b7 cells. Under control conditions, spontaneous glutamate release was minimal and the b3 cell membrane τ was 6.9 ± 2.0 ms (R = 750 ± 200 MΩ, n = 5 cells). Bathing the slice in a solution that contained 0.6 mM glutamate reduced τ to 2.3 ± 0.3 ms (R = 240 ± 90 MΩ). The actual τ under physiological conditions might be lower insofar as the glutamate concentration bathing b3/b7 cells might be higher than 0.6 mM. For comparison, a further simulation based on Figure 7A shows that a 1 ms membrane τ (corner frequency, f_c, equal to 160 Hz) only reduces the b2 cell noise (σ) by about 33% while having little impact on the steady noise in b3 cells. We suggest that membrane filtering alone would be insufficient to overcome the effects of quantal noise in b3/b7 cells if receptors and release sites were closely juxtaposed as they appear to be in b2 cells. Rather, membrane voltage fluctuations in b3/b7 cells are reduced by moving dendritic receptors away from glutamate release sites.

Discussion

Cone terminals receive contacts from bipolar cells at two sites: within invaginations and along the basal membrane. In mammals, a widely held view is that Off bipolar cells exclusively make basal contacts, whereas On bipolar cell dendrites exclusively occupy the central position within invaginations (Hopkins and Boycott, 1997). Consequently, we reasoned that if ribbons, which sit atop invaginations, are the sole sites of release, then all Off bipolar cells should have quantal events that are smeared and attenuated by an extended diffusion path. Unexpectedly, one subtype of Off bipolar cell, the b2, had quantal events that were fast and relatively large. The b2 cell events were comparable in size and shape to events in HCs, the dendrites of which pass close to ribbon release sites. The results suggest that systematic differences in diffusion distance account for the characteristic event shapes in b2, b3, and b7 cells.

Event Shape Is Not Related to Cone-Cone Coupling

Most ground squirrel cones are connected by electrical synapses (the length constant for current spread is ~0.5 cone diameters; DeVries et al., 2002). Consequently, a depolarization in one cone will "inject" current into neighbors, which will then depolarize at a rate determined by their membrane time constants (τ = 5–10 ms). Since neighboring cones frequently contact the same bipolar cell, a cone step depolarization typically produces an immediate, sharp inward current in the postsynaptic bipolar cell that is followed in 5–10 ms by a slow, hump-shaped inward current, which presumably originates in release from neighboring cones.

A number of observations argue against a role for cone coupling in producing the slow EPSCs in b3 and b7 cells. First, b2, b3, and b7 cell dendrites overlap at contacts with 7 to 15 contiguous (i.e., coupled) cones (Li and DeVries, 2006). Consequently, if indirect signaling were to produce slow events in one cell type (e.g., the b3), it should also produce slow events in the other cell types (e.g., the b2 and b7) which are postsynaptic to the same cones. Second, fast and slow EPSCs emerge

from the baseline noise at almost the same time (within ~200 μs; Figures 1–3 and 8) relative to a 1 ms cone depolarization and are not separated by 5–10 ms as predicted by the cone membrane time constant. And third, a series of brief threshold cone depolarizations produced sequences of either fast or slow events in a bipolar cell, but not both. A threshold depolarization in one cone is unlikely to bring neighboring cones to threshold. Thus, cone coupling does not appear to underlie the differences in quantal shape.

Ribbon-Mediated versus Ectopic Release

The conclusion that an individual fusion event can produce the distinctively shaped quantal responses in HCs and Off bipolar cells is based on the assumption that release from different sites in the terminal is unrelated. An alternative view is that cones undergo spontaneous fluctuations in membrane voltage that could coordinate vesicle fusion at multiple sites. However, the close match between the shapes of the predicted and observed peaks in the cross-correlation functions (Figures 3B and 3C and 3E and 3F) argues against a correlating mechanism that involves an underlying voltage change. Changes in voltage would necessarily be slowed by the cone membrane time constant and would impose a longer time course on the shared events.

We did not examine release under conditions of prolonged cone depolarization, which is associated with sustained Ca^{2+} entry, and where ectopic or basal fusion could occur (Zenisek et al., 2003). However, we make two arguments against a major role for ectopic release in cone to bipolar cell signaling under our present recording conditions. First, the existence of correlated events in b2 and b3/b7 cells suggests that transmitter can diffuse from ribbons to basal contacts, so other mechanisms are not needed to explain transmission. And second, the shapes of the correlated and most uncorrelated spontaneous events in a bipolar cell are similar (Figures 3B and 3C and 3E and 3F), which implies that correlated and uncorrelated events come from the same source.

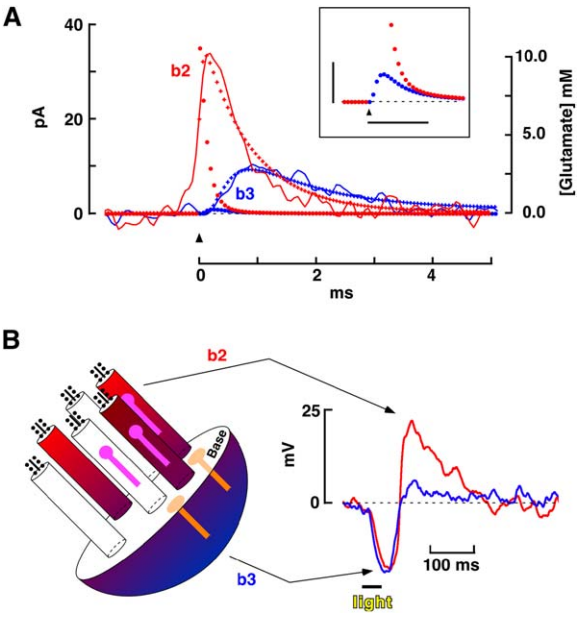

Figure 8. Simulation and Diagram of Signaling in Two Transmitter Microenvironments at the Cone Terminal

(A) Fits (crosses) to spontaneous events recorded simultaneously in a b2 (red) and a b3 cell (blue). Membrane currents (solid lines) are inverted. The glutamate concentrations at the receptors are plotted by circles. The arrow indicates the calculated time of vesicle fusion. (Inset) Enlarged view of a plot of the calculated glutamate concentration at b2 and b3 cell receptors as a function of time. Scale bars, 0.4 mM and 0.5 ms.

(B) (Left) Multiple invaginations (narrow cylinders) open onto the cone base (not drawn to scale). Transmitter concentration is high (red) near the top of an invagination immediately after vesicle fusion. The transition from high to low glutamate concentration, a consequence of spread, is symbolized by the red to blue gradient. b2 cell processes are located within invaginations (purple), and each respond to release from a single ribbon. b3/b7 contacts are located at the base of the terminal where they can sample transmitter from several invaginations. (Right) Membrane voltage in a b2 (red trace) and a b3 (blue trace) cell during a 50 ms flash of light administered to a dark-adapted retinal slice.

Quantal Response Shape and Diffusion Distance

Are the shapes of the quantal responses in b2 and b3/b7 cells consistent with the anatomical distances between cone ribbon release sites and the invaginating and basal contacts of bipolar cells? To address this question, we devised kinetic models for b2 and b3 cell receptors. The models were optimized against receptor properties measured during rapid perfusion experiments (see Experimental Procedures). Once optimized, the kinetic models took as their input a time-dependent glutamate concentration profile that was obtained from a simple equation for the diffusion of a solute from a point source into a hemisphere [Equation (2)]. The kinetic model output was the single channel open probability, P, as a function of time. The model had three free parameters: r, the radial distance between the release site and the receptor cluster; t_0, the time of vesicle fusion [both r and t_0 are components of the diffusion equation, Equation (2)]; and, a scaling factor for P that is related to the number of postsynaptic receptors. The model made a number of simplifying assumptions: (1) A vesicle contains 2500 transmitter molecules [N in Equation (2); ~350 mM; Rao-Mirotznik et al., 1998]; (2) the concentration at the mouth of a vesicle fusion pore rises instantaneously and then declines exponentially with τ = 100 μs; and (3) b2 and b3 cell receptors obey a seven-state reaction scheme (Jonas et al., 1993).

Using the receptor models, we fitted the small evoked events in a b2 cell (Figure 1E), a b3 cell, and, for illustration (because the model was optimized for b3 cells), a b7 cell (Figure 1B). As a more rigorous test, well-defined joint events were selected from simultaneous recordings of spontaneous activity in b2 and b3 (or b3/7) cells and fitted with the additional constraint that the vesicle fusion time be the same. Figure 8A shows the fit to a joint event in a b2 and a b3 cell. For the b2 cell response, the calculated diffusion radius was 0.10 μm, the peak transmitter concentration at the receptor was 10.6 mM, and the peak channel open probability was 0.72. Assuming a single-channel conductance of 20 pS (Lerma, 1999), the number of postsynaptic channels was about 33. For the b3 cell response, the diffusion radius was 0.46 μm, the peak transmitter concentration was 0.3 mM, the peak channel open probability was 0.17, and

the number of postsynaptic channels was 42. The relatively large responses of the two cells in Figure 8A were also fitted by assuming the simultaneous fusion of two vesicles (Singer et al., 2004). The calculated diffusion radii were 0.15 and 0.56 μm for the b2 and b3 cell, respectively. Overall, the fits indicated that b2 cell receptors were located within 0.15 μm of release sites, whereas b3/7 cell receptors were 0.5–1.0 μm from release sites (Table 3). The calculated b2 and b3/b7 receptor distances are consistent with the anatomical distances (Raviola and Gilula, 1975; Calkins et al., 1996).

The fits to b2 spontaneous and small evoked EPSCs decayed more rapidly than could be fitted either with the present model or by using the models and constants of Jonas et al. (1993) and Hausser and Roth (1997). One possibility is that the synaptic receptors saturate during quantal release. In this view, the quantal response decay would be limited by the rate of receptor desensitization, which might be underestimated in our measurements (e.g., Figure 4A). In support of this possibility, cyclothiazide nearly doubled the exponential time constant of spontaneous EPSC decay (n = 2 b2 cells).

Both calculated and observed responses are consistent with the idea that a long extracellular diffusion path shapes events in b3 and b7 cells, whereas b2 cells receive transmitter from nearby release sites. Modeling also suggests that the slow time course of the b3/b7 small EPSC is the combined outcome of a temporally smeared glutamate concentration profile and the slow activation kinetics of b3/b7 receptors when exposed to low concentrations of glutamate.

Table 3. Parameters from Modeling of Small Evoked and Spontaneous EPSCs

	r (μm)[a]	C_{max} (mM)	P_{max}[b]	n
Single cells				
b2	0.08 ± 0.07	2.32 ± 0.60	0.56 ± .07	6
b3	0.92 ± 0.25	0.07 ± 0.06	0.04 ± 0.04	14
b7	0.76 ± 0.07	0.08 ± 0.02	0.05 ± 0.01	6
Pairs				
b2	0.08 ± 0.03	9.53 ± 5.92	0.70 ± 0.08	5
b3	0.77 ± 0.29	0.13 ± 0.14	0.04 ± 0.09	3
b3/7	0.64	0.14	0.05	2

[a] r, radial diffusion distance; C_{max}, peak glutamate concentration; P_{max}, peak open channel probability.
[b] P_{max} of isolated recetors exposed to 4.8 mM glutamate equals 0.8.

Off Bipolar Cell Contacts in Other Mammals

The tips of b3 bipolar cell dendrites colocalized with GluR5 subunit labeling (unpublished data), which is found basally between invaginations (Li and DeVries, 2006). GluR5 labeling is located basally between invaginations in primate (Haverkamp et al., 2001b), cat (Qin and Pourcho, 2001), and rabbit (unpublished data) cones. b7 cells also contacted cones between invaginations, but contact regions were weakly labeled by an antibody to the GluR5 subunit. An antibody to the kainate receptor subunits GluR6/7 did not label in the ground squirrel, but does label basal contacts in the cat (Morigiwa and Vardi, 1999) and primate (Haverkamp et al., 2001b). The results suggest a common architecture in mammals in which the Off bipolar cells that express kainate receptors contact cones in the basal position.

Using light microscopy, we could not distinguish whether b2 dendrites were central or merely semi-invaginating. Nonetheless, based on the similar sizes and shapes of the quantal events in HC and b2 cells, we consider the b2 cell contacts to be "functionally" invaginating. In the current view, mammalian Off bipolar cells avoid the central position in invaginations, and instead contact cones along the basal membrane that extends peripherally from the edges of invaginations (Famiglietti and Kolb, 1976; Kolb, 1979; Hopkins and Boycott, 1997). There is at least one exception to this view: McGuire et al. (1984) serially sectioned a presumptive cat Off bipolar cell, the Cba2, that made only central invaginating contacts. A similar cell was identified as semi-invaginating by Nelson and Kolb (cb1; 1983) and may express AMPA receptors (Morigiwa and Vardi, 1999; Qin and Pourcho, 1999; Pourcho et al., 2002). In the primate, Off bipolar cells rarely made central invaginating contacts, but one type of diffuse bipolar cell, the DB3 (Hopkins and Boycott, 1997), made about 75% of its contacts in the triad associated or semi-invaginating position. The DB3 and b2 cell share many characteristics including calbindin labeling (DeVries, 2000; Jacoby et al., 2000). In sum, there may be at least one type of Off bipolar cell in mammalian retinas that has AMPA receptors and selectively makes central or semi-invaginating contacts with cones.

West (1976) examined the cone contacts of a Golgi-stained b2 cell using electron microscopy and reported them to be exclusively basal. A review of the literature suggests that the currently designated b2 cell (DeVries, 2000; Cuenca et al., 2002) differs from West's b2. West's b2 cell stratifies above the b3 cell and would today be classified as a subset of b7 cell.

Functions of Invaginating and Basal Off Bipolar Cell Contacts

We estimate that vesicles fuse randomly at a rate of 500–1000 s^{-1} at a cone to b2 cell synapse (consisting of 7 ± 3 invaginations; Li and DeVries, 2006) in the dark. A brief light pulse will hyperpolarize a cone for perhaps 50 ms, stopping release. During this interval, depleted vesicle docking sites on the ribbon can refill and postsynaptic AMPA receptors can recover from desensitization. On top of this, the return to the depolarized baseline following the pulse will coordinate release at multiple ribbons. The result is that at light-off there is a sharp increase in the glutamate concentration near fully sensitized b2 receptors, producing a large transient EPSC. It follows that b2 cells should undergo a large transient voltage depolarization after a flash, and indeed this is what is characteristically observed (Figure 8B). It may be that the depolarizing transient is the critical signal for ganglion cells rather than the hyperpolarization. Transient bipolar cells such as the b2 could provide input to transient ganglion cells.

b3 and b7 cell contacts seem poorly suited to generate transient responses at light-off because of their distance from ribbon release sites and prolonged kainate receptor desensitization (DeVries, 2000). Rather, we speculate that b3 and b7 cells use only membrane hyperpolarizations to encode light. In line with expectation, b3 cell membrane voltage was relatively steady in the dark,

smoothly hyperpolarized during a light flash, and returned directly to baseline immediately afterward (Figure 8B). Sustained bipolar cells such as the b3 and b7 could provide input to sustained classes of ganglion cells.

Cone versus Other CNS Synapses

In common with the cone synapse, spillover to glutamate receptors elsewhere in the CNS can occur over distances of 500 nm (Rusakov and Kullmann, 1998). Unlike at the cone synapse, spillover elsewhere is usually associated with high-affinity metabotropic or NMDA receptors or is observed under conditions of reduced transporter glutamate uptake (Asztely et al., 1997; Isaacson, 1999). The results of DiGregorio et al. (2002) provide an important exception to these generalizations. Working at the mossy fiber to granule cell synapse in the cerebellum, they showed that glutamate released from one presynaptic site could activate relatively low-affinity AMPA receptors at distant postsynaptic sites (mean distance = 770 nm). Unlike at the mossy fiber synapse, where spillover occurs after direct transmission, spillover appears to be the prodominant mechanism of transmission at the cone to b3/b7 cell synapse.

Transmission at the cone to b3/b7 cell synapse exemplifies two current ideas about the functions of postsynaptic kainate receptors: kainate receptors are "extrasynaptic" and receive transmitter by spillover; and, kainate receptors integrate synaptic input to provide a tonic depolarization. At the mossy fiber to CA3 pyramidal cell synapse, single or infrequent action potential stimuli activated only AMPA receptors, whereas a tetanic stimulus resulted in a postsynaptic depolarization that was mediated by kainate receptors. The interpretation is that kainate receptors were activated by spillover and thus extrasynaptic (Vignes and Collingridge, 1997; Castillo et al., 1997). At the cone synapse, b2 cell AMPA receptors are the local postsynaptic receptors, whereas the b3 and b7 cell kainate receptors are more distant and effectively "extrasynaptic." The second idea is that kainate receptors function to mediate a tonic depolarization (Frerking and Ohliger-Frerking, 2002). In this view, repeated stimulation is more likely to cause the summation of kainate receptor-mediated EPSCs due to their prolonged time course. Analogously, at the cone basal synapse, a continuous stream of attenuated and smeared events produces a steady bipolar cell current. The mechanisms that produce the steady current in b3 and b7 cells reduce synaptic noise and potentially enhance the reliability of small signal transmission, but at the expense of transmitting large rapid signals, which is instead the task of b2 cells.

Experimental Procedures

The procedures for recording from ground squirrel slices have been described (DeVries and Schwartz, 1999; DeVries, 2000). All animal procedures were approved by the Animal Care and Use Committee of Northwestern University. The external recording solution contained (in mM) 115 NaCl; 3.2 KCl; 1.24 $MgSO_4$; 2 $CaCl_2$; 6 glucose; 2 succinate; 1 lactate; 1 malate; 1 pyruvate; 24 $NaHCO_3$; 0.05 strychnine; 0.05 picrotoxin; pH 7.4 with 5% CO_2/95% O_2. The preparation was superfused (0.2 ml/min) and maintained at 32ºC. The external solution during rapid perfusion experiments contained the following (in mM): 125 NaCl; 3.1 KCl; 1.24 $MgSO_4$; 2 $CaCl_2$; 10 HEPES; pH 7.4 with NaOH. The pipette solution contained the following (in mM): 80 KCl; 30 CsCl; 7 $MgCl_2$; 10 HEPES; 10 BAPTA-K_4; 5 ATP; 0.5 GTP; pH 7.4 with KOH. Slices were visualized with a Zeiss Axioskop FS microscope. Membrane currents, recorded with two or three Axopatch 200B amplifiers (Molecular Devices), were low-pass filtered at 2 or 5 kHz and digitized at 5–16.7 kHz with a ITC-18 acquisition interface (Instrutech) controlled by a Macintosh G4 computer running custom software (Igor 5.0, WaveMetrics). Bipolar cell membrane voltage was maintained at −70 mV. Values are mean ± S.D. TBOA, NBQX, and DNQX were obtained from Tocris. Other chemicals were from Sigma-Aldrich.

Analysis of Spontaneous and Small EPSCs

Bipolar cell pipette noise was reduced by coating with parafilm (American National Can). Holding currents were usually small, and neither series resistance nor pipette capacitance were compensated. Before analysis, traces were filtered in software (a Gaussian filter with f_c = 1250 or 1000 Hz), which limited 20 – 80% rise times to 180 or 220 μs, respectively. Postsynaptic events were evoked by briefly (<1 ms) depolarizing a cone. The amount of transmitter released could be adjusted by changing the size of the depolarization (DeVries and Schwartz, 1999). Cone voltage was controlled in either the whole cell configuration, a "loose seal" configuration (DeVries, 2000), or by permeabilizing a patch of membrane with β-escin (Fan and Palade, 1998). The loose seal configuration was preferred because it minimized rundown during long experiments. Similar quantal event shapes were observed with all three recording techniques.

Event amplitudes and rise times were determined with a custom algorithm (Igor 5.0) that fitted each event with a smooth curve. The fit was critical for determining the rise times of very small, slow events in the presence of noise. These events could not be low-pass filtered, since the same filter would have to be applied to fast events. The fitting algorithm first calculated the average EPSC in a series and then made two passes over the individual trials. The first pass determined whether an event occurred. A threshold was set at three times the noise standard deviation. A copy of the trace was then filtered in software (f_c = 200 Hz). A response was judged to have occurred if the smoothed trace exceeded the threshold at any time during an interval delimited by the length of the average EPSC. The event in the original trace was then fitted [Equation (2)] during the second pass to obtain the 20%–80% rise time and peak amplitude. Alternatively, response failures were fitted in the appropriate interval with a curve that approximated the shape of the average EPSC [Equation (2)] and which could only be scaled in amplitude. No rise information was obtained.

The curve used to fit responses was obtained by convolving the output of a diffusion equation [Equation (2)] with a profile that had a fixed exponential rise (τ = 0.1 ms) and decay (τ equal to either 0.5 or 1.0 ms for fast and slow events, respectively) and which crudely approximated a receptor impulse response. The diffusion equation had an output, *C(t)*, which is a time-dependent concentration, and four free parameters: *N*, which scales the amplitude; *r*, the radial distance between release sites and receptors; t_0, which can

$$C(t) = \frac{N}{(4\pi D(t - t_0))^n} e^{-r^2/4Dt} \qquad (2)$$

be likened to the instant of vesicle fusion; and, the exponent *n*, which provided the best fits when set to 1.5. *D* was fixed at 0.33 $\mu m^2\ s^{-1}$ (Nielsen et al., 2004). Spontaneous events in HC and b2 cells were detected by a simple thresholding procedure and analyzed with standard peak fitting routines in Igor. Spontaneous events in b3 and b7 cells were detected by eye and fitted with Equation (2).

Amplitude histograms were fitted by a sum of five Gaussian profiles. A fit had five free parameters, which included the mean quantal content, location of the Gaussian peak corresponding to failures, the Gaussian width of the failure peak, the event amplitude, and the Gaussian width of the event. For b3 and b7 cells, the peak corresponding to event "failures" was markedly asymmetric, having an increased density of small events along its negative flank. In these cases, a better fit was obtained by using the sum of two five-peak Gaussian profiles, one profile comprised of "small" events and the other of "large" events. The profiles shared the same mean quantal content but differed in event amplitude and width. The fit also determined the fraction of the events that were small (or large).

Rapid Perfusion

Receptor-containing membrane was obtained from slices by excising either the soma with an attached dendrite (DeVries, 2000) or the soma alone. Isolated somas yielded smaller currents, but the recordings were more stable and the solution switching times could be more rapid. The rapid perfusion system used a double-barrel pipette (Vitrocom) mounted on a piezoelectric translator (Burleigh). One barrel of the pipette contained control solution, and the other could be switched among four to five test solutions (switching time ~5 s). Results were accepted only if the receptor response to a maximal glutamate concentration before and after a series was nearly the same. The timing of the solution switch was measured after each experiment by rupturing the bipolar cell and monitoring the junction potential change produced by switching between control and a solution in which 15 mM gluconate anion was substituted for Cl^-. The identity of the recorded bipolar cell was determined by two criteria. First, b2 cells could be distinguished from b3/b7 cells based on soma shape; and second, b3 cell receptors recovered from desensitization more slowly than b7 cell receptors (DeVries, 2000).

Modeling of Receptor Kinetics and Small EPSC Time Courses

Transition rate constants were obtained using the Q-matrix approach (Colquhoun and Hawkes, 1995). Optimization was carried out with a genetic algorithm (Matlab 7.1; Mathworks). Results from a representative b2 and a b3 cell were selected, and the model was optimized against the following parameters: (1) the first 6 ms of the average response to a 4.8 mM step of glutamate scaled to the maximal open probability obtained from a nonstationary fluctuation analysis of the series; (2) steady-state channel open probability in 4.8 mM glutamate; (3) a deactivation time constant of 1.1 ms; (4) the τ for recovery from desensitization (DeVries, 2000); and (5) the EC_{50} and Hill coefficients. The models achieved all the optimization goals and generated responses that approximated the membrane currents during steps into lower concentrations of glutamate, which were not part of the optimization.

The concentration of glutamate at the receptor "cluster" was calculated from Equation (2) with the output, *C(t)*, doubled. The model had three free parameters: t_0, r, and a scaling factor that converted channel open probability into membrane current. The values of these three variables were iteratively changed (Matlab function lsqcurvefit) to minimize the difference between simulated and actual events.

Cell Labeling and Confocal Microscopy

The methods for labeling and imaging cone terminals and bipolar cells have been described (Li and DeVries, 2006). Further details can be found in the Supplemental Data.

Supplemental Data

The Supplemental Data for this article can be found online at http://www.neuron.org/cgi/content/full/50/5/735/DC1/.

Acknowledgments

This work was supported by NIH Grant EY12141 and Research to Prevent Blindness. We thank Dr. Eric Schwartz for early support and Drs. Isabelle Mintz and Joshua Singer for critical reading of the manuscript.

Received: June 22, 2005
Revised: February 22, 2006
Accepted: April 18, 2006
Published: May 31, 2006

References

Ashmore, J.F., and Copenhagen, D.R. (1983). An analysis of transmission from cones to hyperpolarizing bipolar cells in the retina of the turtle. J. Physiol. *340*, 569–597.

Asztely, F., Erdemili, G., and Kullmann, D.M. (1997). Extrasynaptic glutamate spillover in the hippocampus: dependence on temperature and the role of active glutamate uptake. Neuron *18*, 281–293.

Baylor, D.A., and Fuortes, M.G.F. (1970). Electrical responses of single cones in the retina of the turtle. J. Physiol. *207*, 77–92.

Cadetti, L., Tranchina, D., and Thoreson, W.B. (2005). A comparison of release kinetics and glutamate receptor properties in shaping rod-cone difference in EPSC kinetics in the salamander retina. J. Physiol. *569*, 773–788.

Calkins, D.J., Tsukamoto, Y., and Sterling, P. (1996). Foveal cones form basal as well as invaginating junctions with diffuse ON bipolar cells. Vision Res. *36*, 3373–3381.

Castillo, P.E., Malenka, R.C., and Nicoll, R.A. (1997). Kainate receptors mediate a slow postsynaptic current in hippocampal CA3 neurons. Nature *388*, 182–186.

Clements, J.D., Lester, R.A.J., Tong, G., Jahr, C.E., and Westbrook, G.L. (1992). The time course of glutamate in the synaptic cleft. Science *258*, 1498–1501.

Colquhoun, D., and Hawkes, A.G. (1995). A Q-matrix cookbook. In Single-Channel Recording Second edition, B. Sakmann and E. Neher, eds. (New York: Plenum Press), pp. 589–633.

Cossart, R., Epsztein, J., Tyzio, R., Becq, H., Hirsch, J., Ben-Ari, Y., and Crepel, V. (2002). Quantal release of glutamate generates pure kainate and mixed AMPA/kainate EPSCs in hippocampal neurons. Neuron *35*, 147–159.

Cuenca, N., Deng, P., Linberg, K.A., Lewis, G.P., Fisher, S.K., and Kolb, H. (2002). The neurons of the ground squirrel retina as revealed by immunostains for calcium binding proteins and neurotransmitters. J. Neurocytol. *31*, 649–666.

DeVries, S.H. (2000). Bipolar cells use kainate and AMPA receptors to filter visual information into separate channels. Neuron *28*, 847–856.

DeVries, S.H., and Schwartz, E.A. (1999). Kainate receptors mediate synaptic transmission between cones and 'Off' bipolar cells in a mammalian retina. Nature *397*, 157–160.

DeVries, S.H., Qi, X., Smith, R., Makous, W., and Sterling, P. (2002). Electrical coupling between mammalian cones. Curr. Biol. *12*, 1900–1907.

Diamond, J.S., and Jahr, C.E. (1997). Transporters buffer synaptically released glutamate on a submillisecond time scale. J. Neurosci. *17*, 4672–4687.

DiGregorio, D.A., Nusser, Z., and Silver, R.A. (2002). Spillover of glutamate onto synaptic AMPA receptors enhances fast transmission at a cerebellar synapse. Neuron *35*, 521–533.

Dowling, J.E., and Boycott, B.B. (1966). Organization of the primate retina: electron microscopy. Proc. R. Soc. Lond. B Biol. Sci. *166*, 80–111.

Dvorak, C.A., Granda, A.M., and Maxwell, J.H. (1980). Photoreceptor signals at visual threshold. Nature *283*, 860–861.

Eliasof, S., and Werblin, F. (1993). Characterization of the glutamate transporter in retinal cones of the tiger salamander. J. Neurosci. *13*, 402–411.

Fain, G.L., Granda, A.M., and Maxwell, J.M. (1977). Voltage signal of photoreceptors at visual threshold. Nature *265*, 181–183.

Famiglietti, E.V., and Kolb, H. (1976). Structural basis for ON- and OFF-center responses in retinal ganglion cells. Science *194*, 193–195.

Fan, J.S., and Palade, P. (1998). Perforated patch recording with β-escin. Pflugers Arch. *436*, 1021–1023.

Frerking, M., and Ohliger-Frerking, P. (2002). AMPA receptors and kainate receptors encode different features of afferent activity. J. Neurosci. *22*, 7434–7443.

Hausser, M., and Roth, A. (1997). Dendritic and somatic glutamate receptor channels in rat cerebellar purkinje cells. J. Physiol. *501*, 77–95.

Haverkamp, S., Grunert, U., and Wassle, H. (2000). The cone pedicle, a complex synapse in the retina. Neuron *27*, 85–95.

Haverkamp, S., Grunert, U., and Wassle, H. (2001a). The synaptic architecture of AMPA receptors at the cone pedicle of the primate retina. J. Neurosci. *21*, 2488–2500.

Haverkamp, S., Grunert, U., and Wassle, H. (2001b). Localization of kainate receptors at the cone pedicles of the primate retina. J. Comp. Neurol. *436*, 471–486.

Hopkins, J.M., and Boycott, B.B. (1992). Synaptic contacts of a two-cone flat bipolar cell in a primate retina. Vis. Neurosci. *8*, 379–384.

Hopkins, J.M., and Boycott, B.B. (1997). The cone synapses of cone bipolar cells of primate retina. J. Neurocytol. *26*, 313–325.

Isaacson, J.S. (1999). Glutamate spillover mediates excitatory transmission in the rat olfactory bulb. Neuron *23*, 377–384.

Jacoby, R.A., Wiechmann, A.F., Amara, S.G., Leighton, B.H., and Marshak, D.W. (2000). Diffuse bipolar cells provide input to OFF parasol ganglion cells in the macaque retina. J. Comp. Neurol. *416*, 6–18.

Jonas, P., Major, G., and Sakmann, B. (1993). Quantal components of unitary EPSCs at the mossy fibre synapse on CA3 pyramidal cells of rat hippocampus. J. Physiol. *472*, 615–663.

Kolb, H. (1970). Organization of the outer plexiform layer of the primate retina: electron microscopy of Golgi-impregnated cells. Philos. Trans. R. Soc. Lond B. Biol. Sci. *B258*, 261–283.

Kolb, H. (1979). The inner plexiform layer in the retina of the cat: electron microscopic observations. J. Neurocytol. *8*, 295–329.

Lasansky, A. (1973). Organization of the outer synaptic layer in the retina of the larval tiger salamander. Philos. Trans. R. Soc. Lond. B Biol. Sci. *B265*, 471–489.

Lerma, J. (1999). Kainate receptors. In Ionotropic Glutamate Receptors in the CNS, P. Jonas and H. Monyer, eds. (Berlin: Springer), pp. 275–307.

Lester, R.A., Clements, J.D., Westbrook, G.L., and Jahr, C.E. (1990). Channel kinetics determine the time course of NMDA receptor-mediated synaptic currents. Nature *346*, 565–567.

Li, W., and DeVries, S.H. (2006). Bipolar cell pathways for color and luminance vision in a dichromatic mammalian retina. Nat. Neurosci. *9*, 669–675.

Linberg, K.A., Suemune, S., and Fisher, S.K. (1996). Retinal neurons of the California squirrel, *Spermophilus beecheyi*: A Golgi study. J. Comp. Neurol. *365*, 173–216.

Liu, G., Choi, S., and Tsien, R.W. (1999). Variability of neurotransmitter concentration and nonsaturation of postsynaptic AMPA receptors at synapses in hippocampal cultures and slices. Neuron *22*, 395–409.

Maple, B.R., Werblin, F.S., and Wu, S.M. (1994). Miniature excitatory postsynaptic currents in bipolar cells of the tiger salamander retina. Vision Res. *18*, 2357–2362.

Matsui, K., and Jahr, C.E. (2003). Ectopic release of synaptic vesicles. Neuron *40*, 1173–1183.

McGuire, B.A., Stevens, J.K., and Sterling, P. (1984). Microcircuitry of bipolar cells in cat retina. J. Neurosci. *4*, 2920–2938.

Missotten, L. (1965). The Ultrastructure of the Human Retina (Brussels: Arscia, Uitgaven N. V.).

Morigiwa, K., and Vardi, N. (1999). Differential expression of ionotropic glutamate receptor subunits in the outer retina. J. Comp. Neurol. *405*, 173–184.

Nelson, R., and Kolb, H. (1983). Synaptic patterns and response properties of bipolar and ganglion cells in the cat retina. Vision Res. *23*, 1183–1195.

Nielsen, T.A., DiGregorio, D.A., and Silver, R.A. (2004). Modulation of glutamate mobility reveals the mechanism underlying slow-rising AMPAR EPSCs and the diffusion coefficient in the synaptic cleft. Neuron *42*, 757–771.

Pourcho, R.G., Qin, P., Goebel, D.J., and Fyk-Kolodziej, B. (2002). Agonist-stimulated cobalt uptake provides selective visualization of neurons expressing AMPA- or kainate-type glutamate receptors in the retina. J. Comp. Neurol. *454*, 341–349.

Qin, P., and Pourcho, R.G. (1999). Localization of AMPA-selective glutamate receptor subunits in the cat retina: a light- and electron-microscopic study. Vis. Neurosci. *16*, 169–177.

Qin, P., and Pourcho, R.G. (2001). Immunocytochemical localization of kainate-selective glutamate subunits GluR5, gluR6, and GluR7 in the cat retina. Brain Res. *890*, 211–221.

Rao-Mirotznik, R., Harkins, A.B., Buchsbaum, G., and Sterling, P. (1995). Mammalian rod terminal: Architecture of a binary synapse. Neuron *14*, 561–569.

Rao-Mirotznik, R., Buchsbaum, G., and Sterling, P. (1998). Transmitter concentration at a three-dimensional synapse. J. Neurophysiol. *80*, 3163–3172.

Raviola, E., and Gilula, N.B. (1975). Intramembrane organization of specialized contacts in the outer plexiform layer of the retina. A freeze-fracture study in monkeys and rabbits. J. Cell Biol. *65*, 192–222.

Rice, S.O. (1944). Mathematical analysis of random noise. Bell Syst. Tech. J. *23*, *24*, 1–162. Reprinted in Selected Papers on Noise and Stochastic Processes (1954), N. Wax, ed. (New York: Dover).

Rusakov, D.A., and Kullmann, D.M. (1998). Extrasynaptic glutamate diffusion in the hippocampus: ultrastructural constraints, uptake, and receptor activation. J. Neurosci. *18*, 3158–3170.

Sampath, A.P., and Rieke, F. (2004). Selective transmission of single photon responses by saturation at the rod-to-rod bipolar synapse. Neuron *41*, 431–443.

Singer, J.H., Lassova, L., Vardi, N., and Diamond, J.S. (2004). Coordinated multivesicular release at a mammalian ribbon synapse. Nat. Neurosci. *7*, 826–833.

Tong, G., and Jahr, C.E. (1994). Multivesicular release from excitatory synapses of cultured hippocampal neurons. Neuron *12*, 51–59.

Vignes, M., and Collingridge, G.L. (1997). The synaptic activation of kainate receptors. Nature *388*, 179–182.

Wadiche, J.I., and Jahr, C.E. (2001). Multivesicular release at climbing fiber-Purkinje cell synapses. Neuron *32*, 301–313.

West, R.W. (1976). Light and electron microscopy of the ground squirrel retina: functional considerations. J. Comp. Neurol. *168*, 355–377.

West, R.W., and Dowling, J.E. (1975). Anatomical evidence for cone and rod-like receptors in the gray squirrel, ground squirrel, and prairie dog retinas. J. Comp. Neurol. *159*, 439–460.

Zenisek, D., Davila, V., Wan, L., and Almers, W. (2003). Imaging calcium entry sites and ribbon structures in two presynaptic cells. J. Neurosci. *23*, 2538–2548.